Numerical Simulation of Underwater Blast-Wave Focusing Using a High-Order Scheme

S. M. Liang* and H. Chen†
National Cheng-Kung University, Tainan 701, Taiwan, Republic of China

I. Introduction

THE problem of underwater blast-wave focusing over truncated ellipsoidal reflectors is considered. Namely, a blast wave is initiated, which will be propagating into a quiet water when time evolves. The truncated ellipsoidal reflector has a ratio (a/b) of the half major axis (a) to the half minor axis (b) and a ratio (r/b) of the aperture radius (r) to the half minor axis b. The flow feature of this problem is nonlinear shock-wave focusing and negative pressures. Negative pressures represent tensile waves. Blast-wave focusing can produce a maximum (positive) pressure and a minimum (negative) pressure. The negative pressures may result in a cavitation phenomenon. The cavitation has negative effects on tissue damages[1] and may have a positive effect on stone comminution because of the induced microjets[2,3] in the application of extracorporeal shock-wave lithotripsy for treating human calculi. Past researchers' studies indicated that the minimum (negative) pressure is about 20% in magnitude of the maximum pressure.[2] To our knowledge no paper has reported an accurate prediction of the maximum pressure, negative pressures, and the ratio of the minimum pressure to the maximum pressure.

In 1995 Jiang and Shu[4] introduced a fifth-order weighted essentially nonoscillatory (WENO) scheme in Cartesian coordinates and validated the scheme on various test problems involving linear and nonlinear hyperbolic equations. Their results indicated that the WENO scheme seems to be able to resolve some discontinuities and complicated flow structures. Therefore we extend the WENO scheme to a curvilinear coordinate system. In the past 10 years researchers have used a piecewise linear method,[5] a random choice method,[6] and a total variation diminishing (TVD) scheme.[7] For the problem of underwater shock-wave focusing, these schemes seemed to have difficulties with the accurate prediction of the maximum pressure and negative pressures without special numerical techniques such as grid adaption. Thus in this study an attempt is made to develop a high-order Euler solver using the fifth-order WENO scheme for simulating the axisymmetric blast-wave focusing problem.

II. Mathematical Formulation

Neglecting the effects of viscosity and bubbles caused by negative pressure, the governing equations for the flow of underwater shock-wave focusing are the time-dependent Euler equations:

$$\frac{\partial Q}{\partial t}+\frac{\partial F}{\partial x}+\frac{\partial G}{\partial y}+H=0$$

$$Q=\begin{bmatrix}\rho\\ \rho u\\ \rho v\\ E\end{bmatrix},\qquad F=\begin{bmatrix}\rho u\\ \rho u^2+p'\\ \rho uv\\ (E+p')u\end{bmatrix}$$

$$G=\begin{bmatrix}\rho v\\ \rho uv\\ \rho v^2+p'\\ (E+p')v\end{bmatrix},\qquad H=\frac{\alpha}{y}\begin{bmatrix}\rho v\\ \rho uv\\ \rho v^2\\ (E+p')v\end{bmatrix} \tag{1}$$

where Q is the conserved variables; F, G are the flux vectors; H is the source term caused by axisymmetry; ρ is the density; $p(=p'-B)$ is the pressure; u and v are the velocity components; and c is the speed of sound, E the total energy per unit volume, and B a constant. The modified pressure p' is related to the flow variables E, u, v:

$$E=\frac{p'}{\gamma-1}+\frac{\rho(u^2+v^2)}{2} \tag{2}$$

where the values of γ and B are chosen as 7.66 and 2955 bars, respectively, such that the speed of sound $c=(\gamma p'/\rho)^{1/2}$ at room temperature is 1483 m/s. Note that the equation of state for water has been adopted, which is described by the modified Tait equation. For detail, refer to the paper of Sommerfeld and Müller.[5] Note that Eq. (1) represents a planar flow for $\alpha=0$ and an axisymmetric flow for $\alpha=1$. For easy treatment of boundary conditions, the governing equations are usually written in the body-fitted coordinate (ξ, η). Thus Eq. (1) becomes

$$\frac{\partial \hat{Q}}{\partial t}+\frac{\partial \hat{F}}{\partial \xi}+\frac{\partial \hat{G}}{\partial \eta}+\hat{H}=0 \tag{3}$$

The relation between Eqs. (1) and (3) is expressed by

$$\hat{Q}=\frac{Q}{J},\qquad \hat{F}=\frac{\xi_x F+\xi_y G}{J}$$

$$\hat{G}=\frac{\eta_x F+\eta_y G}{J},\qquad \hat{H}=\frac{H}{J}$$

where $J=\xi_x\eta_y-\xi_y\eta_x$ is the Jacobian.

III. Numerical Method

A. WENO Scheme

The numerical method of high-order accuracy in a finite volume approach is used to solve Eq. (3). For time integration a fourth-order Runge–Kutta method is employed. For spatial discretization a fifth-order WENO scheme is adopted. For more detail, refer to Refs. 4, 8, and 9. A local time step is chosen for all unsteady flow calculations. The Courant number is set to be 0.5. All computations were performed on a DEC alpha workstation with a 256-MB memory.

B. Initial and Boundary Conditions

An initial blast wave[5] is prescribed by

$$p(r)=p_l+(p_h-p_l)\exp[-(r_0-r)/c\tau],\qquad r\le r_0$$

where r is the distance from the blast center, which is assumed to be the first focus of the ellipsoidal reflector, c the sound speed in water, τ the wave decaying time, p_h the pressure at the wave front, and p_l the pressure ahead of the blast wave. Initially, the flow properties are determined by the given pressure ratio $p(r)/p_l$ based on the Rankine–Hugoniot conditions. As shown in Fig. 1, the boundary condition on the reflector surface is the slip condition. At the outflow/inflow and top boundaries, the nonreflecting boundary condition of Thompson[10] is specified, and a symmetry boundary condition is imposed on the bottom boundary.

IV. Results and Discussion

A. Code Validation

Case 1: Shock-tube problem. A shock tube with a pressure ratio of 10 is tested. The working fluid is air. The diaphragm is located at $x=0.8$. The computational domain is chosen to be $\{(x, y) \mid -0.815\le x\le 2.445,\ 0\le y\le 0.0455\}$. A uniform 300×100 grid was used. The computed result of the Mach number distribution at (dimensionless) time $t=0.55$ is shown in Fig. 1, which is compared with the exact solution and the solution obtained by a TVD scheme.[10] One can see that the three solutions are in good agreement. In particular, the WENO scheme has a better resolution at the discontinuities, the shock wave and contact surface, than the TVD scheme.

Case 2: Simple underwater shock-wave reflection problem. Consider a normal shock with pressure ratio of 700 impinging on a plane wall located at $x=0$. The working fluid is water. The pressure ratio

Received 29 September 1998; revision received 11 March 1999; accepted for publication 5 April 1999.

*Professor, Department of Aeronautics and Astronautics. Associate Fellow AIAA.
†Graduate Student, Department of Aeronautics and Astronautics.

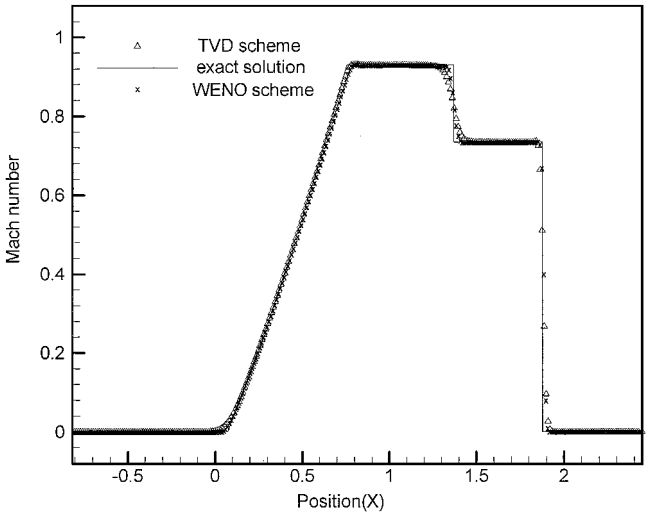

Fig. 1 Mach number distribution for a shock-tube problem, $t = 0.55$.

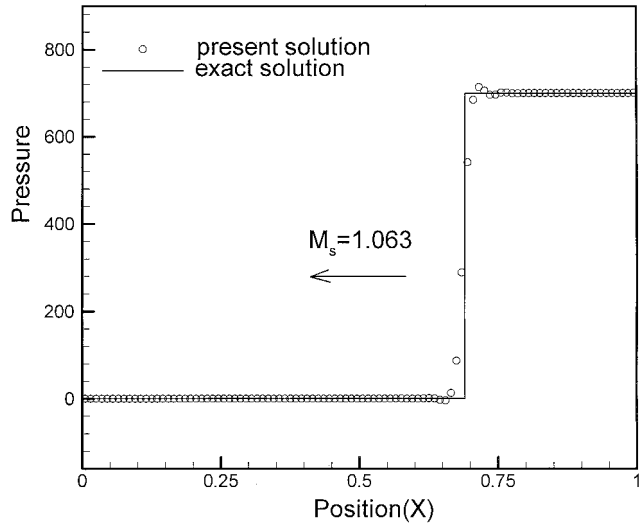

a) Incident shock at $t = 0.001$

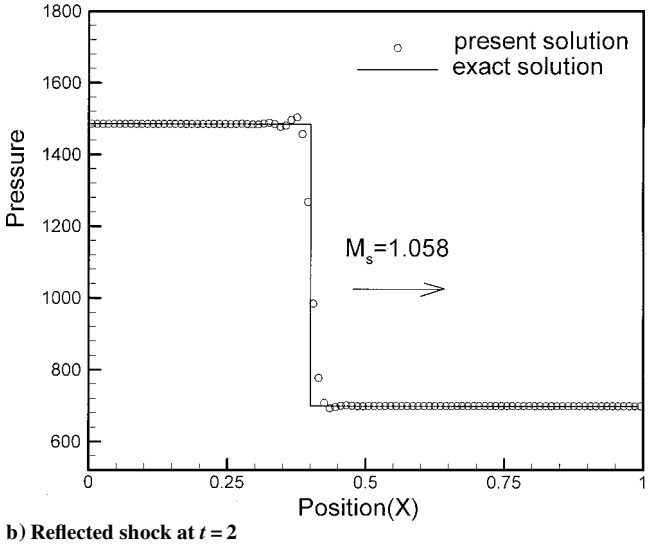

b) Reflected shock at $t = 2$

Fig. 2 Simple underwater shock-wave reflection problem.

produces an incident shock Mach number of 1.063. From analysis, the pressure ratio for the reflected shock wave with a Mach number of 1.058 is 2.119 or 1483.33/700. The same grid as in case 1 was used. The computed pressure ratio for the reflected shock is 2.122 or 1485.6/700. The relative error is only 0.033%. Figure 2 shows the pressure distributions at $t = 0.001$ and 2. From Fig. 2a one can see that there is a slight oscillation near the incident and reflected shock waves.

Case 3: Underwater shock-wave focusing over a parabolic reflector. Consider a two-dimensional parabolic ($y = 4fx$) reflector with a ratio of the focal length f to the half aperture length l equal to 0.357. We set $l = 1$ unit and $f = 0.357$ units. Initially, a normal shock with pressure ratio of 700/1 is given and is incident to the reflector. The computational domain used is chosen to be $\{(x, y) \mid 0 \le x \le 1.7, 0 \le y \le 1\}$, which is similar to the one indicated in Fig. 1, but the top boundary was set to be a wall boundary. Five grids—100 × 100 (grid 1), 150 × 150 (grid 2), 200 × 200 (grid 3), 200 × 250 (grid 4), 200 × 300 (grid 5)—were used. The variation of the maximum pressures on these five grids is shown in Fig. 3. The maximum pressure is increased with the grid number. The improvements on the maximum pressure are respectively about 23, 16, 6, and 2%, when the grid is sequentially changed from grid i to grid $i + 1$, $i = 1, 2, 3, 4$. Notice that the increase in the maximum pressure is

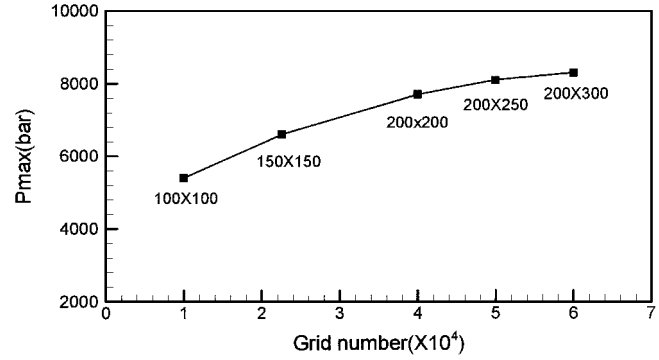

Fig. 3 Comparison of maximum pressures along the symmetry axis.

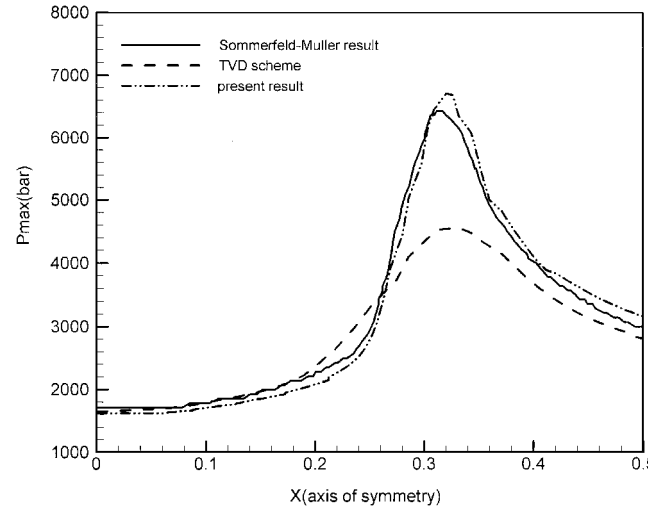

Fig. 4 Effect of grid number on the maximum pressure.

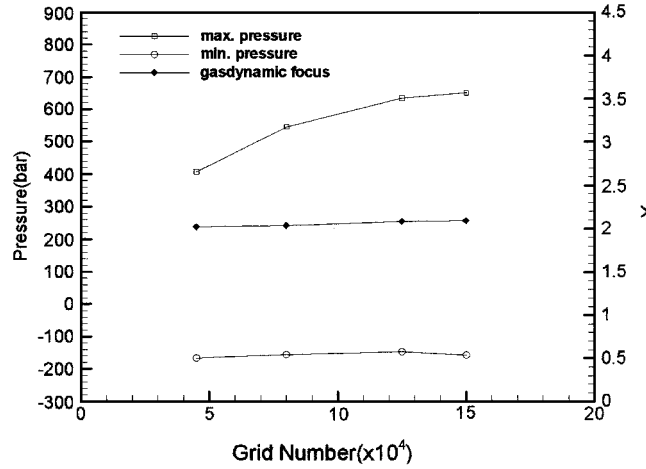

Fig. 5 Effects of grid number on the maximum pressure, the minimum pressure, and the gasdynamic focus.

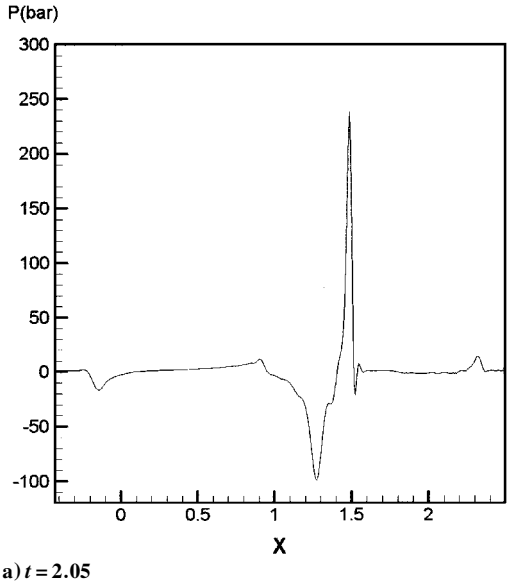

a) $t = 2.05$

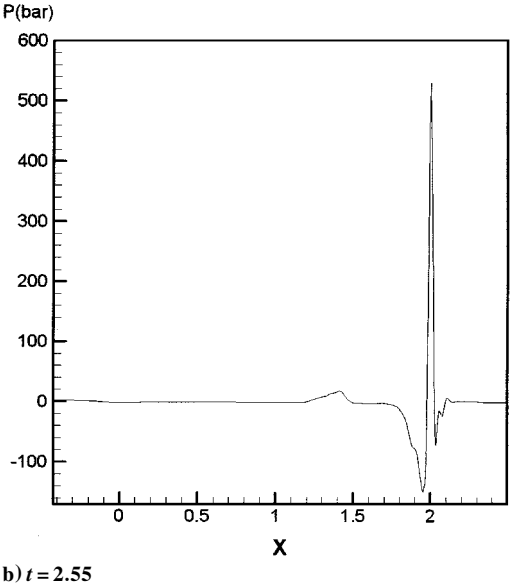

b) $t = 2.55$

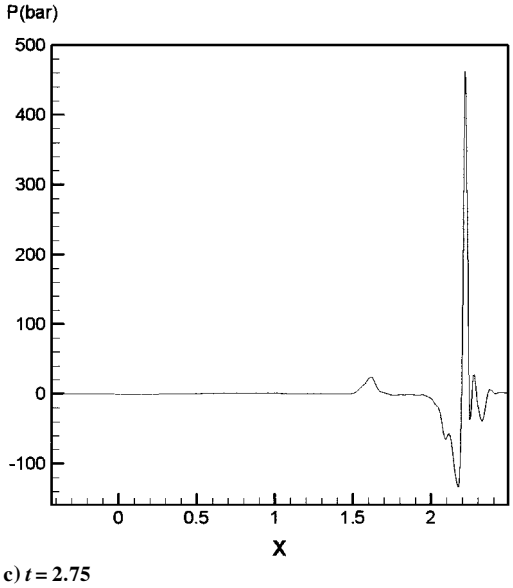

c) $t = 2.75$

Fig. 6 Pressure distributions along the symmetry axis at different instants.

slowed down when the grid number is greater than 200×200. The problem was also studied by Sommerfeld and Müller.[5] Their numerical solution on a grid with grid size of $\Delta x = 0.01$ is compared to our solution on grid 2, because grid 2 has grid sizes close to 0.01. The computed maximum pressures along the x axis are shown in Fig. 4 and compared with the results obtained by a TVD scheme.[11] The TVD scheme underpredicts the pressure peak, which occurred at the gasdynamics focus, $x = 0.32$. Moreover, the present solution is reasonably close to the result of Sommerfeld and Müller.

B. Axisymmetric Blast-Wave Focusing Problem

The geometry of the truncated ellipsoidal reflector is given by $x^2/a^2 + y^2/b^2 = 1$ with $a/b = 1.4$ and $r/b = 0.95$, where a, b are the half major and minor axes and r the aperture radius of the reflector. The parameter values of the blast wave are chosen to be $r_0 = 0.3$, $\tau = 0.04$, $p_l = 1$ bar, and $p_h = 200$ bars. We choose the focal length f as the characteristic length and redefine the first focus as the coordinate origin, and so the first and second foci are located at $x = 0$ and 2, respectively. The computational domain is chosen to be $\{(x, y) \mid -0.4289 \le x \le 2.5, 0 \le y \le 0.9696\}$. To study the effect of grid number used on the numerical solution, four grids were used. They are the 300×150 grid (grid 1), the 400×200 grid (grid 2), the 500×250 grid (grid 3), and the 500×300 grid (grid 4). Figure 5 shows the variations of the minimum and maximum pressures and their ratios on different grids. Note that the computed gasdynamic foci are also included. The improvement on the maximum (positive) pressure is approximately 35% for changing grid 1–2, 13% for changing grid 2–3, and 3% for changing grid 3–4. The improvement on the minimum pressure because of sequential grid change is approximately 7, 6, and −5%, respectively. The ratios of the minimum pressure to the maximum pressure are 61% on grid 1, 29% on grid 2, 24% on grid 3, and 25% on grid 4, respectively. Sturtevant[2] pointed out that the ratio from lithotriptor data is about 20%, which means that the present pressure predictions are reasonably accurate. The computed gasdynamic focus is approximately $x = 2.02$ on grid 1, 2.03 on grid 2, 2.08 on grid 3, and 2.09 on grid 4, respectively. The computed gasdynamic foci are very close to the geometric focus, which is the theoretical gasdynamic focus based on the linear acoustic theory. Figure 6 shows the numerical result of the pressure distributions along the symmetry axis at different instants. Figure 6a indicates that the reflected blast wave has not focused yet. Figure 6b shows that the reflected blast wave is in focusing, resulting in a maximum pressure and a minimum pressure. After wave focusing the pressure peaks are reduced, as shown in Fig. 6c. From Fig. 6 one can see that the negative pressures because of fast expansion always occur closely behind the maximum pressure. The negative pressures represent tensile stresses and may induce a cavitation phenomenon in a real situation when it is below a critical value.

V. Conclusion

A high-resolution numerical solver of the Euler's equations with air or water as a working fluid has been developed. The numerical scheme is a fourth-order Runge–Kutta method for time integration and a fifth-order WENO scheme for spatial discretization on a curvilinear coordinate. The solver is validated on four test problems. For the axisymmetric underwater blast-wave focusing problem, the computed maximum and minimum pressures seem to be reasonably accurate.

Acknowledgments

The support for this study under National Science Council Contracts NSC 86-2212-E-006-061 and NSC 86-2622-E-006-004 is gratefully acknowledged.

References

[1] Delius, M., "Medical Applications and Bioeffects of Extracorporeal Shock Waves," *Shock Waves*, Vol. 4, No. 2, 1994, pp. 55–72.

[2] Sturtevant, B., "Shock Wave Physics of Lithotriptors," *Endourology*, edited by A. D. Smith et al., Vol. 2, Quality Medical Publishing, Inc., St. Louis, MO, 1996, pp. 530–552.

[3] Timita, Y., Obara, T., Takayama, K., and Kuwahara, M., "Cavitation Phenomena in Extracorporeal Microexplosion Lithotripsy," *Shock Waves*, Vol. 3, No. 3, 1994, pp. 149–157.

[4]Jiang, G. S., and Shu, C. W., "Efficient Implementation of Weighted ENO Schemes," *Journal of Computational Physics*, Vol. 126, No. 1, 1996, pp. 202–228.

[5]Sommerfeld, M., and Müller, H. M., "Experimental and Numerical Studies of Shock Wave Focusing in Water," *Experiments in Fluids,* Vol. 6, No. 3, 1998, pp. 209–216.

[6]Olivier, H., and Grönig, H., "The Random Choice Method Applied to Two-Dimensional Shock Focusing and Diffraction," *Journal of Computational Physics*, Vol. 63, No. 1, 1986, pp. 85–106.

[7]Isuzugawa, K., and Horiuchi, M., "Experimental and Numerical Studies of Blast Wave Focusing in Water," *Proceedings of the 18th International Symposium on Shock Waves*, Vol. 1, Springer–Verlag, New York, 1992, pp. 347–350.

[8]Shu, C. W., Zang, T. A., Erlebacher, G., Whitaker, D., and Osher, S., "High-Order ENO Schemes Applied to Two- and Three-Dimensional Compressible Flow," *Applied Numerical Mathematics*, Vol. 9, No. 1, 1992, pp. 45–71.

[9]Liu, X. D., Osher, S., and Chan, T., "Weighted Essentially Non-Oscillatory Schemes," *Journal of Computational Physics*, Vol. 115, No. 1, 1994, pp. 200–212.

[10]Thompson, W., "Time Dependent Boundary Conditions for Hyperbolic Systems," *Journal of Computational Physics*, Vol. 68, No. 1, 1987, pp. 1–24.

[11]Liang, S.-M., Tsai, C.-J., and Wu, L.-N., "Efficient, Robust Second-Order Total Variation Diminishing Scheme," *AIAA Journal,* Vol. 34, No. 1, 1996, pp. 193–195.

M. Sichel
Associate Editor

Diode-Laser Sensor for Velocity Measurements in Hypervelocity Flows

S. D. Wehe,* D. S. Baer,† and R. K. Hanson‡
Stanford University, Stanford, California 94305-3032

Introduction

REFLECTED shock tunnels have been used to provide high-enthalpy hypersonic flowfields for ground-testing applications for about 40 years.[1] High-velocity flow in these tunnels is generated from the conversion of the enthalpy in the tunnel reservoir to directed motion (kinetic energy) of the gas through a steady expansion process via a nozzle. The freestream conditions for the expanded flow are typically calculated from nonequilibrium multidimensional nozzle codes,[2,3] generally based on input from side-wall pressure and shock-speed measurements near the shock tube end wall. Experimental determinations of the freestream conditions and the steady-state test time have been very limited and generally indirect, and there have apparently been no previous diagnostics capable of time-resolved velocity measurements. This Note describes the development and implementation of a compact sensor, based on absorption spectroscopy techniques and comprising tunable diode lasers and fiber optics, that capitalizes on the natural presence of chemically frozen atomic potassium (K) for the direct determination of gas velocity from measurements of Doppler-shifted absorption line shapes. The large line strength of the probed potassium transition ($^2S_{1/2} \rightarrow {}^2P_{1/2}$) near 770 nm allows the determination of velocity from absorption measurements of trace concentrations (either naturally present or intentionally seeded) over path lengths of a few centimeters. The compact sensor (containing the optoelectronics for direct absorption measurements) was inserted into the flowfield to provide velocity measurements with relatively high spatial resolution.

Received 29 January 1999; revision received 12 April 1999; accepted for publication 21 April 1999. Published by the American Institute of Aeronautics and Astronautics, Inc., with permission.

*Research Assistant, High Temperature Gasdynamics Laboratory, Department of Mechanical Engineering.

†Research Associate, High Temperature Gasdynamics Laboratory, Department of Mechanical Engineering.

‡Professor, High Temperature Gasdynamics Laboratory, Department of Mechanical Engineering.

Diagnostic Description

The diode laser sensor was applied to measure velocity in the Calspan 96-in. hypersonic shock tunnel. The operational details and capabilities of the facility have been published previously.[4] The design of this second-generation sensor is conceptually similar to that of a larger probe developed previously for simultaneous near-infrared (1.3–1.4 μm) H_2O absorption measurements of temperature, species concentration, and velocity in hypersonic flows.[5,6] Figure 1 shows the layout of the optoelectronics within the probe. The probe was installed directly into the flowfield, 25 cm below the nozzle centerline, to minimize complications due to boundary layers and facility vibration. The nozzle exit diameter is 121 cm. The probe walls were constructed with 1.6-mm thick stainless steel for structural integrity. No cooling was required due to the short flow times.

The wavelength of the (AlGaAs) diode laser was current tuned at a 10-kHz repetition rate over the potassium D_1 ($^2S_{1/2} \rightarrow {}^2P_{1/2}$) transitions near 770 nm to record a Doppler-shifted absorption feature every 0.1 ms. The laser linewidth ($\Delta\nu_{\text{laser}} = 150 \pm 10$ MHz) was measured with a high finesse ($F = 50$ and free spectral range = 2 GHz at 770 nm) confocal Fabry–Perot interferometer. The optical output (nominal power = 9mW) of the laser was split (60:40) by a cube beam splitter (with a near-infrared antireflection coating) into two beams. The higher intensity beam was coupled into a single-mode (4.5-μm core diameter) fiber and directed 30 m through a hardened conduit to the probe. The lower intensity beam was directed through the confocal interferometer. The transmission through the interferometer was recorded with a silicon photodetector (10-MHz bandwidth) and was used to convert the signal from the time domain to the laser frequency domain. All of the voltage signals were acquired at a sampling rate of 5 MHz (0.2 μs/point) with 12-bit resolution.

Inside the probe, the laser light was divided by a cube beam splitter into two beams that were directed from one probe finger to the other at a 43.8-deg angle (Doppler-shifted beam) and a 90-deg angle (non-Doppler-shifted beam) with respect to the bulk gas velocity. Wedged (1 deg) windows were mounted in the probe to minimize etalon effects. The laser transmission intensities (~0.3 mW/mm^2) were monitored with silicon photodetectors (2.3-MHz bandwidth) inside the probe. A number 29 Wratten filter (long-pass cutoff wavelength = 630 nm) was affixed to the inside of the upper window, that is, on the receiving finger of the probe in Fig. 1, served to exclude detection of background emission.

Gas velocity was determined from the measured absorption line shapes using the Doppler relation, which relates the measured spectral shift $\Delta\nu$ (in gigahertz), at laser frequency ν, to the gas velocity V_{gas} (in meters per second):

$$\Delta\nu/\nu = V_{\text{gas}}(\cos\theta/c) \tag{1}$$

where c is the speed of light in meters per second and θ is the angle between the beam and the bulk gas velocity. The absorption measurement recorded in situ over a path perpendicular to the bulk-flow direction affords a simple means of nulling the possible effect of pressure shift in the recorded line shapes.

The theoretical basis for determining species concentration from measured absorption spectra is well established.[7,8] The K concentration was determined from the application of Beer's law:

$$-\int_{-\infty}^{\infty} \ell n\left(\frac{I_\nu}{I_\nu^0}\right) \mathrm{d}\nu = SP_iL \tag{2}$$

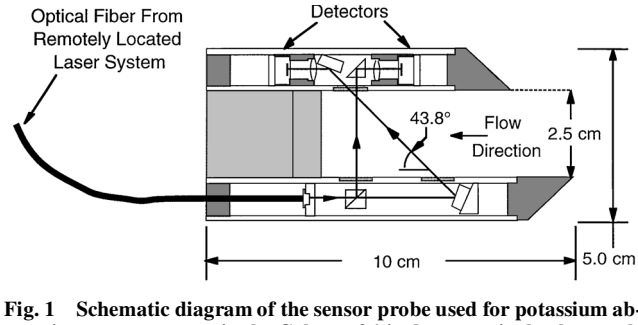

Fig. 1 Schematic diagram of the sensor probe used for potassium absorption measurements in the Calspan 96-in. hypersonic shock tunnel.